Modeling of Bubble Expansion-Induced Cell Mechanical Profile in Laser-Assisted Cell Direct Writing

Wei Wang

Gang Li

Yong Huang[1]
e-mail: yongh@clemson.edu

Department of Mechanical Engineering,
Clemson University,
Clemson, SC 29634

Cell damage due to the mechanical impact during laser-assisted cell direct writing has been observed and is a possible hurdle for broad applications of fragile cell direct writing. The objective of this study is to numerically investigate the bubble expansion-induced cell mechanical loading profile in laser-assisted cell direct writing. Some conclusions have been drawn as follows. The cell velocity increases initially and then smoothes out gradually with a constant ejection velocity. Both the cell acceleration and pressure can be very high at the beginning period of bubble expansion and then quickly approach zero in an oscillation manner. A high viscosity can lead to an observable velocity increment at the initial stage, but the ejection velocity decreases. The pressure magnitude decreases when the cell-bubble distance is large, and a larger initial pressure induces a larger cell pressure as expected. This study serves as a foundation to further investigate the cell damage mechanism in laser-assisted cell direct writing to improve the effectiveness and efficiency of cell direct writing techniques. [DOI: 10.1115/1.4000101]

1 Introduction

Biomaterial direct-write technologies are being favored as rapid prototyping innovations in the areas of tissue engineering, regenerative medicine, and biosensor/actuator fabrication based on computer-aided designs (CADs). Direct-write technologies include any techniques or processes capable of depositing, dispensing, or processing different types of materials over various surfaces. During a typical direct-write approach, patterns or layered structures are built directly using a CAD design without the use of masks, allowing rapid prototyping of three-dimensional constructs. Among the available direct-write technologies, inkjet and laser-based technologies have been most pioneered to precisely position both nonviable and viable biological patterns and constructs over different substrates [1] under noncontact, maskless, and low temperature conditions.

Laser-assisted cell direct writing technique has been obtaining more and more attention in different biomaterial direct writing applications [2–5] since it does not have any specific viscosity requirements as ink-jetting methods do. Unlike ink-jetting or manual spotting techniques, the laser-assisted process delivers small volume of biomaterials without the use of an orifice, thus eliminating potential clogging issues and enabling diverse classes of biomaterials to be deposited. During a typical laser-assisted cell direct writing, focused highly energetic laser pulses are directed through the backside of the quartz support, over which the cell-based biomaterial is coated. These pulses are then absorbed by either a laser-absorbing matrix of the biomaterial coating (as in matrix-assisted pulsed-laser evaporation direct-write (MAPLE DW)) or a specific laser-absorbing energy conversion layer between the quartz support and the coating to be transferred (as in biological laser printing (BioLP)). Once the laser-absorbing material absorbs most of the laser pulse energy, it forms a bubble due to localized heating in the immediate vicinity of the energy-absorbing material, which is the same for both MAPLE DW and BioLP. Finally, this sublimation releases the remaining coating as a droplet from the interface by ejecting it away from the quartz support to the movable receiving substrate underneath, to form two- or three-dimensional structures by controlled droplet deposition. It should be pointed out that the laser-assisted cell direct writing process discussed here is jet-based, and it is different from the laser guidance direct writing process, which uses laser optical force to guide and move biomaterials [6,7].

In order to commercially implement the different direct-write technologies in the healthcare industry, some biomanufacturing issues need to be carefully addressed. However, manufacturing process-induced damage to cells, especially fragile mammalian cells, still poses a significant challenge to achieve a perfect post-transfer cell viability. The aforementioned cell direct writing process can be divided into two main stages: (1) The cell droplets are formed and ejected due to the laser energy converted momentum and (2) the cell droplets land onto a receiving substrate after traveling through a writing height [1]. During the above two stages, the cells may undergo a severe mechanical deformation, which poses a potential mechanical damage to the cells by making cell membrane permeable [8] or even membrane rupture. The process-induced cell damage must be carefully addressed for cell direct writing to be a viable technology. It has been observed that the post-transfer cell viability can be improved from 50% to 95% in laser printing a fragile cell by changing the substrate hydrogel coating thickness from 20 μm to 40 μm [3]. The landing-induced mechanical profile in cell direct writing has been recently studied [1]; however, the ejection-induced cell mechanical profile must be studied and the associated cell damage must be modeled accordingly.

The objective of this study is to numerically investigate the bubble expansion-induced cell mechanical profile during the laser-assisted cell ejection process. Either Lagrangian or Eulerian mesh has been applied for different computational domains to model this cell mechanical profile using a finite element method (FEM)-based approach. This paper is organized as follows. First, modeling of bubble expansion is reviewed. Second, necessary material models are introduced. To validate the modeling accuracy of the FEM method, the simplified Rayleigh bubble dynamics model-based approach is implemented in an infinite domain to bench-

[1]Corresponding author.

Contributed by the Manufacturing Engineering Division of ASME for publication in the JOURNAL OF MANUFACTURING SCIENCE AND ENGINEERING. Manuscript received September 4, 2008; final manuscript received July 28, 2009; published online September 24, 2009. Editor: Kornel F. Ehmann.

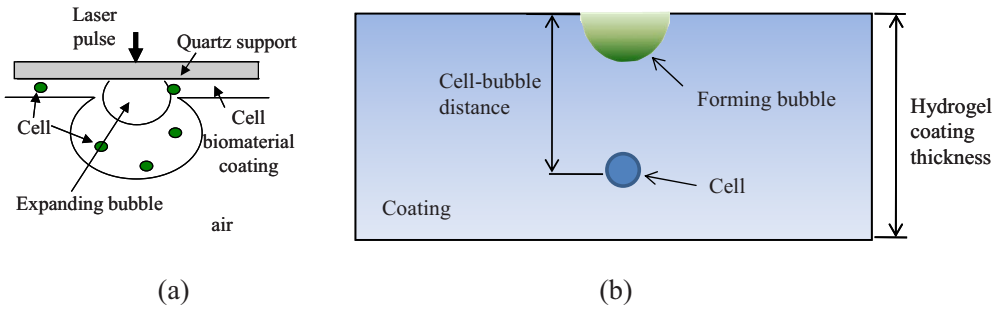

Fig. 1 (*a*) Cell direct writing schematic and (*b*) modeling domain for the bubble expansion-induced cell deformation

mark the FEM method in modeling the cell velocity due to the bubble expansion. The validated FEM method is further applied to study the cell mechanical profile such as velocity, acceleration, and pressure during bubble expansion, and the effects of coating viscosity, cell-bubble distance, and initial bubble pressure on the cell pressure are also studied. Finally, the main conclusions are drawn for better cell direct writing process optimization. This study serves as a foundation for further cell damage investigation in various jet-based cell direct-write technologies as they all deal with the interactions between cells and the surrounding medium during the cell droplet formation process.

2 Background

Two mechanisms are possibly responsible for cell damage during ejection in laser-assisted cell direct writing: the bubble expansion-induced stress wave and the thermoelastic stress wave [9]. The bubble expansion-induced cell mechanical deformation is of interest since it is the dominant effect in laser-assisted cell direct writing. In laser-assisted cell direct writing, upon the absorption of laser pulse energy, the matrix material of the biomaterial coating or the material of/near the energy conversion layer is first vaporized into gaseous phase products and may be further ionized into plasma, forming a nucleus in the cell-based biomaterial coating along the quartz support interface. The formed nucleus evolves into an expanding bubble, and the bubble expansion-induced pressure ejects the surrounding coating material away, forming cell droplets. Since the expansion of the gas bubble is inhibited by the surrounding medium, the confining effect results in significant higher pressure and temperature than those due to ablation in a gaseous environment [9]. When the laser-induced stress transients possess a sufficiently short rise time, their propagation may result in the formation of a shock wave [9,10].

Laser-induced bubble formation and expansion in different media such as living tissues has been of modeling interest since it was observed [9–15]. Once a nucleus is formed upon absorbing the laser pulse energy, the bubble expansion process and its mechanical effect on the surrounding medium can be generally modeled in two approaches: analytically and numerically. The analytical approach is mainly based on the Rayleigh bubble dynamics model [16] and its modified versions such as the Gilmore bubble dynamics model [12–14] to consider the effect of compressible medium and/or include the effect of different medium material properties. However, the analytical approach generally ignores the complexity of material models and it is good for one-dimensional (1D) problems. Alternatively, the finite difference/finite element-based numerical approach has also been applied to capture the one- or two-dimensional bubble expansion process and its mechanical effect [12,15]. The numerical method allows the consideration of complex bubble and medium geometry, as well as enables the application of more realistic material models, which are difficult to be implemented using the analytical approach. The finite element-based approach is also favored in this study for its modeling flexibility.

In the case of laser-assisted cell direct writing, the interactions among the expanding bubble and the surrounding cells are of interest in addition to the bubble expansion dynamics modeling. The mechanical effect of the general bubble expansion on the cell stress and velocity has been studied by applying the Rayleigh bubble dynamics model to model the bubble expansion and the bubble-induced flow field method to estimate the cell mechanical profile [16]; however, the whole modeling process and material models are oversimplified for the sake of an analytical solution. To better elucidate the effect of laser-induced bubble expansion on cell damage in laser-assisted cell direct writing, this study investigates the cell mechanical profile due to the bubble expansion process using the FEM approach to accommodate the large deformation and cell-medium interaction, and it is expected that the modeled mechanical profile information will help reveal the cell damage mechanism in laser-assisted cell direct writing.

3 Computational Modeling and Its Validation

3.1 Problem Statement and Assumptions. Figure 1 shows the schematic of the laser-induced bubble formation and expansion in a typical laser-assisted cell direct writing setup (MAPLE DW). While the MAPLE DW schematic is shown here, the proposed modeling approach is still applicable to BioLP by assuming the energy conversion thickness (usually less than 100 nm) negligible. During the bubble expansion process after the bubble is formed, the high pressure pulse and/or shock wave are generated, which interact with the cells inside the hydrogel-based cell coating medium. It should be pointed out that the coating medium can be any materials other than hydrogel, which it is commonly used. To model the effect of the bubble expansion on the cells during the cell droplet ejection process, the following assumptions are introduced.

1. The formed bubble geometry, temperature, and pressure right after the material thermal evaporation and/or optical breakdown process are assumed known, and the bubble is modeled as the gaseous phase [10,14]. Also, the gas diffusion and further evaporation of biomaterials during the bubble expansion are also ignored.
2. Energy loss due to heat conduction is negligible during the bubble expansion process, and the bubble expansion always moves faster than the speed of heat diffusion [2,13].
3. The bubble gas maintains a constant mass, and the gas gain or loss due to the surrounding material evaporation and the gas diffusion through the bubble wall is negligible [10].
4. The cell coating includes only a cell, which is directly beneath the center of laser pulse.
5. The initial bubble is semispherical.
6. Since the Froude number (a dimensionless number compar-

ing the inertial and gravitational forces) is very large (on the order of 10^7), the gravitational effect is neglected.
7. Surface tension is not considered. During the ejection process, the Weber number (a dimensionless number comparing the inertial effect to the surface tension effect) is high (on the order of $10^2 \sim 10^4$), so the effect of surface tension on the cell deformation and motion may be negligible. For the detailed cell droplet formation simulation, the surface tension should also be carefully considered in the future study.

The FEM approach is implemented in LS-DYNA to study the cell mechanical profile during ejection here with a different mesh for different computational domains, respectively. In this study, four materials, vaporized bubble gas, air, hydrogel (coating material), and cell, are utilized within the computational domain, and Secs. 3.2.1–3.2.4 briefly introduce the material models adopted for each material. The cell is modeled as a solid type material using the Lagrangian mesh for its straightforward and fast implementation, while the bubble, coating medium, and air are modeled using the Eulerian mesh to avoid any extreme element distortion of these materials during ejection. The Lagrangian domain overlaps over the Eulerian domain while the different Eulerian domains share nodes on the common boundaries. The cell/hydrogel interaction is modeled using the appropriate Euler/Lagrange coupling option (all directions coupling method as in LS-DYNA) to capture the viscosity effect within the cell boundary layer, and the interaction among the hydrogel, bubble gas, and air is modeled by defining these materials in multimaterial grouping.

3.2 Material Models. The complete definition of a transient nonlinear dynamics problem requires materials models that define the relationships among the flow variables (pressure, mass density, energy density, temperature, etc.). Sections 3.2.1–3.2.4 briefly introduce the material models of four materials, vaporized bubble gas, air, hydrogel, and cell of the computational domain. These relations generally involve an equation of state, a constitutive equation, and a failure criterion for each constituent material. The numerical simulation is implemented using LS-DYNA 971, and all the material parameters defined in the remainder of the section are available in the LS-DYNA material library [17].

3.2.1 Vaporized Bubble Gas. In laser-assisted cell direct writing, the laser energy-absorbing material along the cell coating-quartz interface (as in MAPLE DW) or of/near the energy conversion layer (as in BioLP) evaporates upon the absorption of laser pulse energy and may further ionize, forming a bubble within the confined coating domain. For simplicity, the bubble gas is modeled as an ideal gas with an equation of state defined as follows:

$$P_b = \rho_b (C_{P-V} - C_{V-V}) T_b \tag{1}$$

where P_b is the bubble pressure, ρ_b is the current mass density, T_b is the temperature, and C_{P-V} and C_{V-V} are defined as the specific heat with respect to the constant pressure and constant volume for the bubble gas, respectively. When the bubble expands, both the density and temperature vary as the bubble volume changes, so does the bubble pressure. The pressure at the initial state (P_{b0}) is defined by the initial mass density and temperature (ρ_{b0} and T_{b0}) as follows:

$$P_{b0} = \rho_{b0} (C_{P-V} - C_{V-V}) T_{b0} \tag{2}$$

Since the bubble gas is a gaseous material and has no ability to support either the shear stress or the negative pressure, no failure model is adopted for the bubble gas.

3.2.2 Air. As the bubble expands, the expanding bubble applies a pressure wave over the cell coating beneath. The cell coating is pushed toward the surrounding air and consequently forms a cell droplet. In the computational analysis, an Eulerian computational domain is used to model the surrounding air, and the air equation of state is modeled as follows:

$$P_a = (\gamma_A - 1) \frac{\rho_a}{\rho_{a0}} E_a \tag{3}$$

where P_a is the air pressure, $\gamma_A = C_{P-A}/C_{V-A}$ is the air constant pressure specific heat over the constant volume specific heat, ρ_a is the current air mass density, ρ_{a0} is the mass density at the reference state, and E_a is the air internal energy per unit reference volume. Since the air pressure and temperature are much smaller than those of the bubble, the air initial internal energy is set as zero for simplicity. Since air is a gaseous material and has no ability to support either the shear stress or the negative pressure, no failure model is adopted for air.

3.2.3 Hydrogel. Natural and synthetic hydrogels contain water within a three-dimensional network of polymer chains [18]. By their nature, hydrogels are highly swollen fluidlike solids, which are water swollen, cross-linked, hydrophilic polymers. Due to their biocompatibility and the ease of their synthesis, the gels have been already extensively used as cell culture and proposed for a wide range of biomedical applications [19,20]. The properties of a particular hydrogel are highly dependent on its structure characteristics, constitutes, and chemical environment [21,22], and some hydrogel mechanical property characterization studies have also been performed [23–25]. However, the knowledge of mechanical properties of hydrogel is still under the development stage.

Equation of state of hydrogel is expected to provide a hydrodynamic material model by which the hydrogel volumetric strength can be determined. Mie–Grüneisen equation of state, as shown in Eq. (4), is used to define the equation of state of hydrogel to consider the compressibility [17]:

$$P_h = \frac{\rho_{h0} C^2 \mu \left[1 + \left(1 - \frac{\gamma_0}{2} \right) \mu - \frac{a}{2} \mu^2 \right]}{\left[1 - (S_1 - 1)\mu - S_2 \frac{\mu^2}{\mu + 1} - S_3 \frac{\mu^3}{(\mu + 1)^2} \right]} + E_h (\gamma_0 + a\mu) \tag{4}$$

where P_h is the hydrogel pressure, C is the intercept of the U_s-U_p curve (sound velocity) as the U_s axis, U_s is the speed of a shock-wave through the material, U_p is the speed of the shocked material, S_1, S_2, and S_3 are the coefficients of the slope of the U_s-U_p curve, γ_0 is the Grüneisen gamma, E_h is the internal energy per initial volume, and a is the first order volume correction to γ_0; the compression μ is defined as $(\rho_h/\rho_{h0}) - 1$, and ρ_h and ρ_{h0} are the density and initial density. The Mie–Grüneisen equation is typically determined based on material parameters c, S_1, S_2, S_3, and γ_0 as specified by LS-DYNA [17]. In this study, since water is the dominant component of hydrogel, the parameters for water are used to define the hydrogel equation of state to simplify the problem.

Since the hydrogel demonstrates fluidlike behavior during large deformation, for simplicity, the null material provided by the LS-DYNA material library [17] is used as the hydrogel constitutive model. When using the null material model, the pressure and deviatoric stress are decoupled. The pressure is determined by the equation of state as Eq. (4), and the deviatoric stress is calculated based on the strain rate and viscosity as follows:

$$\sigma^D = 2\eta \dot{\varepsilon}^D \tag{5}$$

where η is the hydrogel viscosity, σ^D is the deviatoric stress, and $\dot{\varepsilon}^D$ is the deviatoric strain rate. In addition, the cutoff pressure is used to control the hydrogel failure by allowing the hydrogel to numerically cavitate when hydrogel undergoes dilatation (tensile negative pressure) above a certain value, which is usually zero or a small negative value for liquid-type materials.

3.2.4 Cell. During the bubble expansion-induced cell ejection process, the cells undergo complex dynamic pressure and velocity variations, eventually forming the cell droplets. In order to model

the complexity of cell structure and compositions, numerous cell constitutive models have been developed to characterize mechanical responses of living cells subject to both transient and dynamic loads [26]. Generally, cell models can be considered on two levels, macroscopic continuum approaches and microscopic structural approaches. The continuum approaches aim to investigate the overall behavior of cells while microscopic structural approaches focus on the effect from the local component deformation of cells.

Among the continuum approaches, the hyperelastic formulation, neo-Hookean model, has been widely used by some researchers in modeling the cells and biological materials since it can well capture the cell nonlinear large deformation [27,28]. The neo-Hookean model is also used as the cell is modeled as a generic one here, and the cell strain energy potential is described as follows:

$$U = C_{10}(\bar{I}_1 - 3) + \frac{1}{D_1}(J-1)^2 \tag{6}$$

where U is the strain energy potential, C_{10} is dependent on the shear modulus G_0 as $C_{10}=G_0/2$, D_1 is dependent on the initial bulk modulus K_0 as $D_1=2/K_0$, $\bar{I}_1$ is the first deviatoric strain invariant, and J is the determinant of the deformation gradient. The Cauchy stress tensor can be determined based on the second Piola–Kirchhoff stress tensor, which can be calculated by taking the partial differentiation of the strain energy potential with respect to the Green–Lagrange strain tensor. The cell pressure is determined based on the mean stress of the Cauchy stress. As the cytoplasmic membrane, cell wall, and internal structure of a cell may play an important role in determining the cell mechanical profile during ejection, future modeling study should also include the effect of cell biological structure.

Since the goal of this study is to study the companying cell mechanical profile during the cell ejection, the cell failure is not of interest here and the predicted mechanical profile values are not compared with the failure threshold values of any cells. Instead, this study is a foundation for future cell damage/failure modeling in laser-assisted cell direct writing.

3.3 FEM Approach Validation Using the Rayleigh Approach. The FEM approach for cell ejection modeling is first validated before implementation. In this study, it is validated by comparing its modeling performance with that of the classical Rayleigh bubble dynamics model-based approach in capturing the cell velocity due to the bubble expansion in an infinite incompressible medium. For this validation study, the hydrogel coating medium of Fig. 1 is assumed infinite.

The Rayleigh bubble dynamics model [29] is often used to study the response of surrounding incompressible flow to the expansion of a single spherical bubble. The equation for this gas bubble expansion within a hydrogel medium is described as follows:

$$\ddot{R}R + \frac{3}{2}\dot{R}^2 = \frac{1}{\rho_h}(p_i(t) - p_\infty(t)) - \frac{1}{\rho_h}\left(\frac{2\sigma}{R} + \frac{4\eta\dot{R}}{R}\right) \tag{7}$$

where R is the current gas bubble radius, $\dot{R}$ is the first order derivative of R, $\ddot{R}$ is the second order derivative of R, t is the time, $p_\infty(t)$ is the pressure in the hydrogel flow at the infinite distance from the gas bubble, $p_i(t)$ is the pressure inside the bubble, and σ is the surface tension. When the pressure inside the bubble is significantly larger than the pressure introduced by the bubble wall surface tension, the surface tension effect is negligible. Then Eq. (7) can be further reduced to

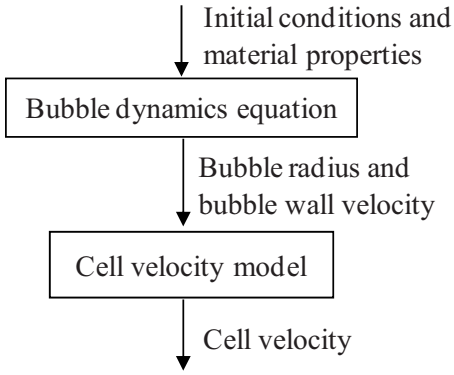

Fig. 2 Computational flow chart of bubble dynamics equation

$$\ddot{R}R + \frac{3}{2}\dot{R}^2 = \frac{1}{\rho_h}(p_i(t) - p_\infty(t)) - \frac{4\eta\dot{R}}{\rho_h R} \tag{8}$$

where the gas pressure inside the bubble $p_i(t)$ is assumed to obey an isentropic law as follows:

$$p_i(t) = p_0(R_0/R)^{3\gamma} \tag{9}$$

where p_0 is the initial bubble gas pressure, γ ($\gamma=1.4$) is the ratio of the specific heat with respect to the constant pressure and constant volume, and R_0 is the initial bubble radius.

The flow velocity $u(r,t)$ at a distance r from the bubble center can be obtained based on the flow incompressibility:

$$u(r,t) = \frac{R^2}{r^2}\dot{R} \tag{10}$$

If the cell deformation is negligible (this simplification is only for this validation case) and the cell volume is also ignored in modeling, the cell center velocity can be approximated as follows:

$$u_{\text{cell}} = \frac{R^2}{d^2}\dot{R} \tag{11}$$

where u_{cell} is the cell (center) velocity and d is the cell-bubble distance.

The computational flow chart of the Rayleigh approach is shown in Fig. 2 and Eq. (8) can be solved using the Runge–Kutta routine. The output of interest of the above Rayleigh model-based approach is the cell velocity, which is to be compared with that from the FEM approach.

To better compare with the results using the Rayleigh model-based approach, the cell deformation should be modeled negligible in the FEM implementation since the Rayleigh model was developed by neglecting the effect of cell deformation. This is achieved by modeling the cell using a linear elastic material model with an artificially high Young modulus of 1.79 GPa (10^3 times higher than that commonly adopted [1]).

In this validation study, the coating medium is assumed incompressible, so a linear polynomial equation of state is selected for the hydrogel coating to make it behave incompressible in this validation study. This equation of state is as follows:

$$P = C_0 + C_1\mu + C_2\mu^2 + C_3\mu^3 + (C_4 + C_5\mu + C_6\mu^2)E \tag{12}$$

where the coefficients μ and E are defined similarly as in Eq. (4). The incompressible approximation of hydrogel can be achieved by setting C_1 as 150 GPa while others C_i ($i=0$, 2, 3, 4, 5, and 6) are zero. The hydrogel cutoff pressure is set as zero in this case.

The other material properties and computational parameters are as follows: the bubble gas specific heats (C_{P-V} and C_{V-V}) are taken as 2.080 J/g K and 1.485 J/g K, respectively, the initial hydrogel coating density (ρ_{h0}) is 1000 kg/m^3, and the hydrogel viscosity (η) is 12×10^{-3} Pa s. The cell-bubble distance is

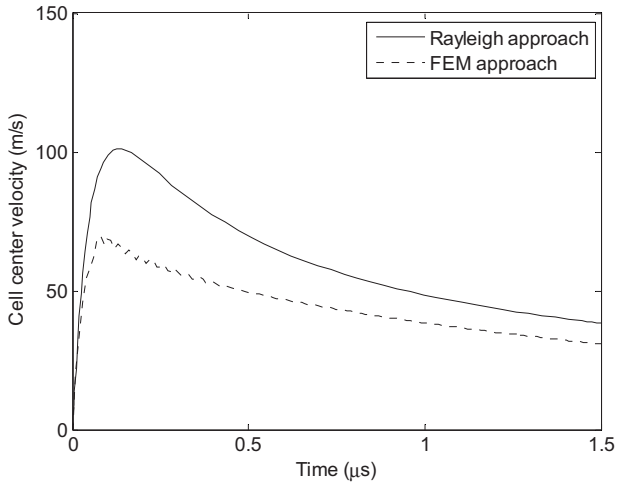

Fig. 3 Cell center velocity comparison under a 221 MPa initial bubble pressure

50 μm. The validation case has been performed under an initial bubble gas pressure (P_{b0}) of 221 MPa, which is picked as one order higher than the bubble pressure in a similar laser-assisted surgery process [30] to simulate the possible effect of vaporization and/or plasma formation. This initial pressure value is equivalent to an initial bubble gas density (ρ_{b0}) of 574.08 kg/m^3 and an initial bubble gas temperature (T_{b0}) of 647 K based on Eq. (2). For the implemented FEM computational domain, 186,330 solid elements are used for the hydrogel coating medium ($500\times500\times500$ μm^3), 1380 solid elements for the bubble gas ($R_0=24$ μm), and 108 solid elements for the cell (6 μm radius). The top surface of the coating is set as the symmetric boundary, and the other surfaces are set as free.

Figure 3 shows the modeling results using both the Rayleigh and FEM approaches. It can be seen that the both approaches lead to similar velocity estimations. Since the hydrogel coating is assumed incompressible, the cell instantaneously moves once the gas bubble expands. The reason that the FEM approach underestimates the cell velocity may be attributed to two reasons: (1) The hydrogel cannot be modeled as perfectly incompressible, which leads to more energy dissipation during the bubble expansion in the FEM implementation, and (2) Eq. (11) of the Rayleigh approach tends to overestimate the cell velocity since both the cell deformation and volume are ignored. This velocity difference is found to be less pronounced under higher initial bubble pressures. The observed velocity oscillation in using the FEM approach is attributed to the elasticity of cell.

Generally speaking, the FEM approach can well capture the bubble expansion-induced cell velocity, and it is expected that the FEM approach should also well capture the cell deformation given proper material models. Compared with the Rayleigh approach, the FEM approach can better model the realistic cell ejection process without unnecessary assumptions on the cell deformation and cell volume as the Rayleigh approach does.

4 Numerical Study of Cell Mechanical Profile

4.1 Model Implementation. The discussed FEM approach is further implemented to study the cell mechanical profile upon the gas bubble expansion during cell ejection. Since the problem described in Fig. 1 is axisymmetric, a quarter of the computational model is analyzed. Figure 4 shows a representative quarter symmetric model for this analysis: a quarter cylinder with a radius of 100 μm and a height of 100 μm represents the hydrogel coating, a semisphere with a radius of 24 μm denotes the initial bubble gas phase, and a spherical cell with a radius of 6 μm is embedded in the center line of cylinder and 55 μm (cell-bubble distance) away from the center of bubble. The air domain is partially shown in Fig. 4. Larger coating domains have also been implemented; however, there is negligible difference in terms of simulation results. A total of 50,318 solid elements are used in which 108 elements for the cell, 11,330 elements for the coating, 37,500 elements for the air, and 1380 elements for the bubble gas. Element 1, the closest to the expanding bubble, represents the top surface region, Element 2 represents the middle region, and Element 3 represents the bottom surface region.

A rigid wall boundary condition is used to model the rigid quartz support. To reduce the effect of reflection of the stress waves at the outer surface of the hydrogel and air domains, a nonreflecting boundary condition is applied for the faces associated with these domains. The nonreflecting boundary condition enables the propagation of pressure waves across the boundaries mimicking an infinitely large coating domain.

The aforementioned material models are applied here. If not especially specified, the same material properties and computational parameters used in Sec. 3 are used here too. The hydrogel cutoff pressure is set as 25 kPa [1,24]. The cell shear modulus is set as 15.6 kPa [27], the Poisson ratio is set as 0.475, and the density is set as 1000 kg/m^3, which are used to estimate C_{10} and D_1. The initial air mass density (ρ_{a0}) is specified as 1.28 kg/m^3, and the initial bubble gas pressure is specified as 221 MPa.

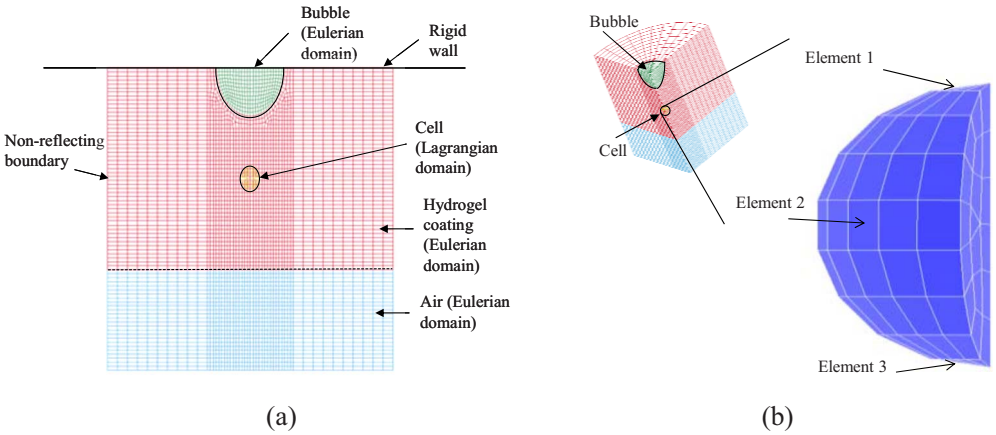

Fig. 4 (*a*) Coupled Lagrangian and Eulerian computational domains and (*b*) distribution of cell elements

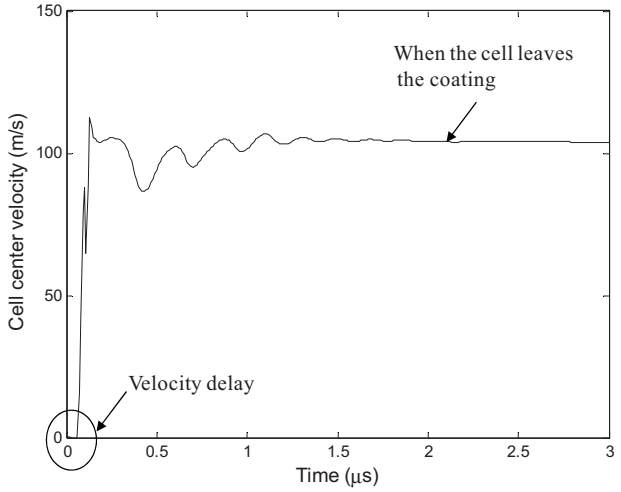

Fig. 5 Evolution of cell center velocity

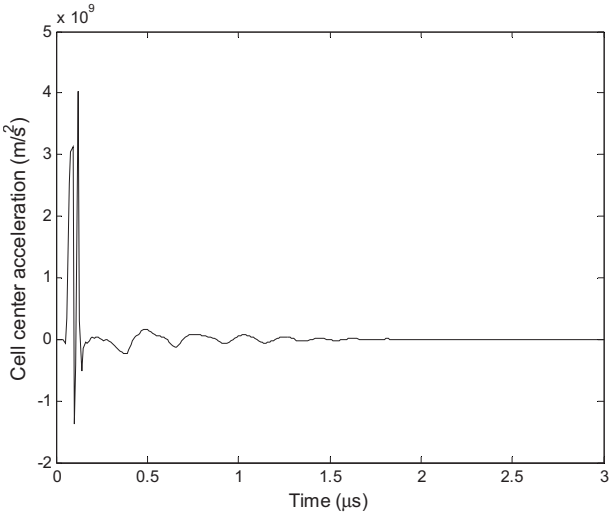

Fig. 6 Evolution of cell center acceleration

4.2 Mechanical Profile of Cell. In order to appreciate the cell mechanical profile such as the cell center velocity, cell center acceleration, and pressure changes during the bubble expansion-induced ejection, some representative simulation results are presented in the following based on the condition of a 221 MPa initial bubble pressure and a 55 μm cell-bubble distance. Such cell mechanical information will help better understand and model cell damage during laser-assisted cell direct writing.

4.2.1 Evolution of Cell Center Velocity and Acceleration. The ejection velocity of cell droplet is of importance in determining the cell viability during the subsequent cell droplet landing process as studied in Ref. [1]. The ejection velocity is the initial velocity at which the cell droplet impacts the receiving substrate. For some applications, the cell droplet ejection velocity should be well controlled to minimize the possible cell damage during landing. Figure 5 shows the cell center velocity evolution during the ejection process. It can be seen that the cell velocity oscillates initially and then smoothes out gradually with a constant ejection velocity (107 m/s in this simulation), and this velocity oscillation is attributed the elasticity of cell, implying a negative acceleration. Due to the compressibility of hydrogel, there is a delay in the velocity response to the bubble expansion, as seen from Fig. 5. After around 2 μs, the cell droplet has a very weak connection with the coating and starts to leave the hydrogel coating with a constant velocity.

Figure 6 shows the simulation result of cell acceleration. As seen from Fig. 6, the cell first accelerates as high as 10^9 m/s^2 at the beginning period of bubble expansion and then quickly approaches zero in an oscillation manner. The high acceleration period only lasts a very short period (about 0.1 μs), and the very short duration is critical to guarantee the cell survival. The absolute magnitude of acceleration depends on the material properties of the hydrogel and cell as well as the initial bubble gas pressure.

4.2.2 Evolution of Pressure. The transferred cells are easily damaged during cell manipulation especially when being subject to the high pressure induced by the stress waves [8]. The stress waves may make the cell membrane permeable, and the molecules in the extracellular medium diffuse into the cytoplasm under the concentration gradient. Subsequently, the plasma membrane reseals to keep the exogenous molecules inside the cell, which may lead to functional cell injury. On the other hand, the stress may induce the cell membrane or other cell components structurally broken, which also can cause cell damage. For this ejection process, the cell pressure due to the bubble expansion should be carefully understood.

Figure 7 shows the simulation result of cell pressure at different cell internal regions. Generally speaking, the pressure can be as high as 10 MPa at the beginning period of bubble expansion and quickly decreases to zero in an oscillation manner, as seen from the cell acceleration evolution in Fig. 6. At a specified moment, the top surface region (Element 1 of Fig. 4(*b*)), which is close to the expanding bubble, experiences the highest pressure level, followed by the bottom surface region (Element 3) and the middle region (Element 2).

4.3 Parametric Study. For the cell damage control during cell direct writing, the effect of typical controllable process conditions such as the coating viscosity, cell-bubble distance, and initial bubble pressure needs to be carefully studied to minimize the possible cell damage while maintaining process efficiency. Since the top surface region of cell (Element 1) usually experiences a relatively severe pressure condition as discussed before, Element 1 is selected as the representative cell region to study the effect of the coating viscosity, cell-bubble distance, and initial bubble pressure on the cell pressure. For this parametric study, only the initial bubble gas density (ρ_{b0}) is changed to 57.408 kg/m^3, which is determined based on a 22.1 MPa initial

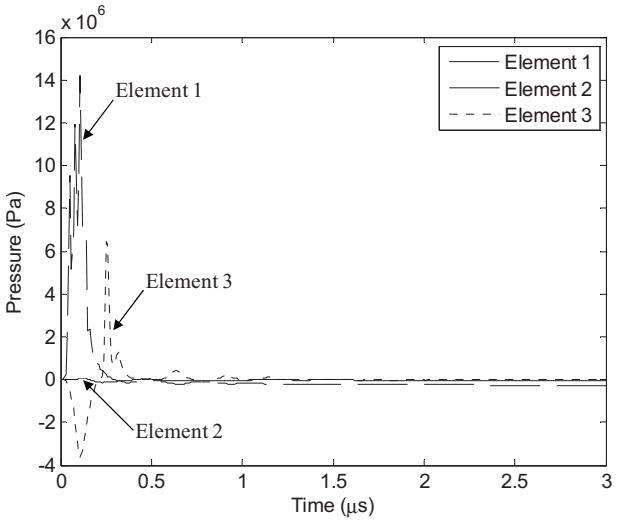

Fig. 7 Cell pressure at different cell internal regions

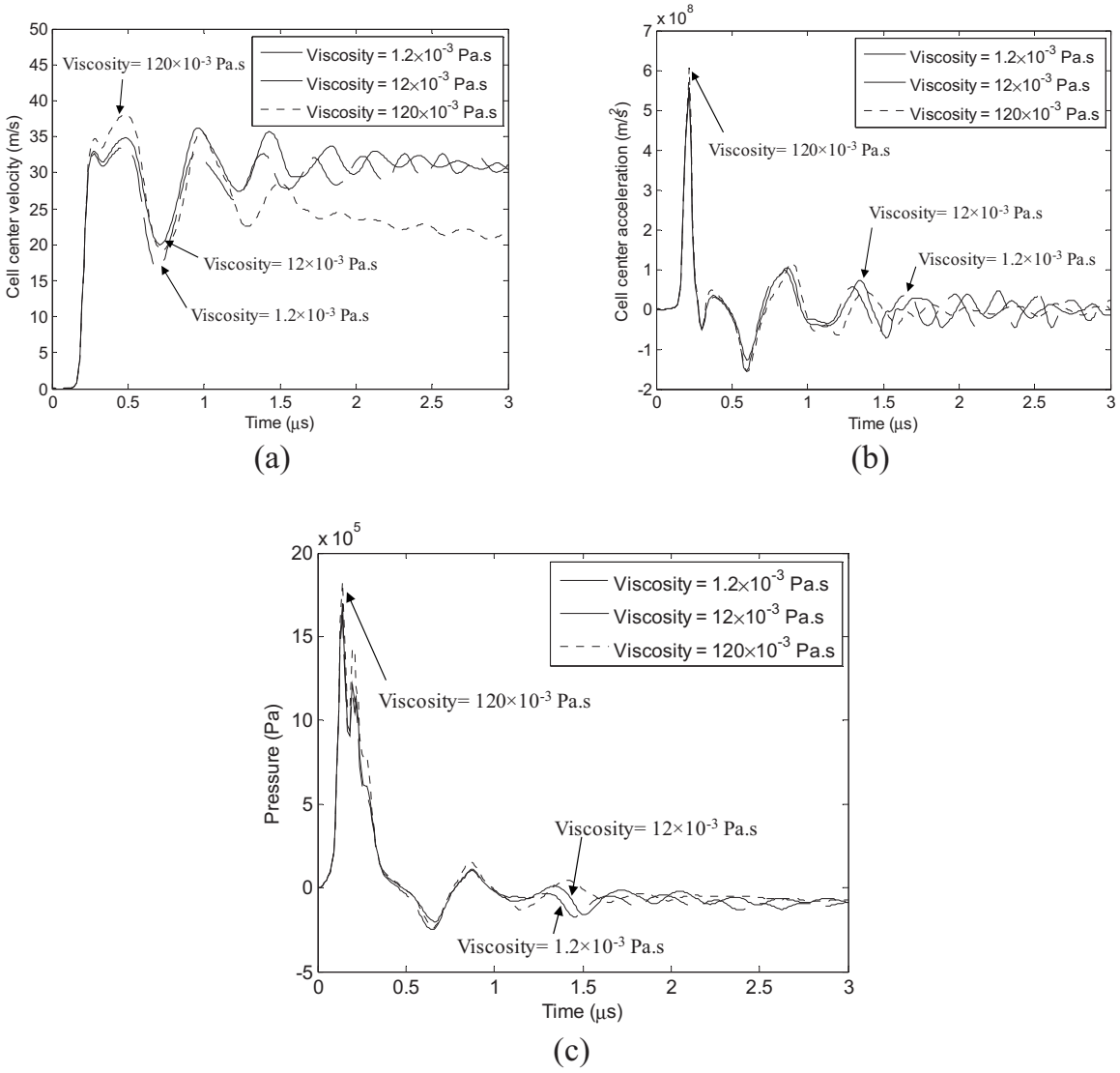

Fig. 8 (*a*) Cell center velocity, (*b*) cell center acceleration, and (*c*) cell pressure under different coating viscosity conditions (the initial pressure is 22.1 MPa and the cell-bubble distance is 55 μm)

bubble pressure. For the sake of simulation efficiency, the 22.1 MPa pressure is selected based on the critical pressure of water as in a previous study [30].

4.3.1 Effect of Coating Viscosity. Figure 8 shows the effect of coating viscosity on the cell center velocity, cell center acceleration, and pressure under the initial pressure of 22.1 MPa and the cell-bubble distance of 55 μm. Three different viscosity values (1.2×10^{-3} Pa s, 12×10^{-3} Pa s, and 120×10^{-3} Pa s) have been studied, and these values are also close to the viscosity of various glycerol solutions, which are gaining widely applications in biological printing [5]. It is shown that there is a small difference between the results using the viscosities of 1.2×10^{-3} Pa s and 12×10^{-3} Pa s; however, the simulation using the viscosity of 120×10^{-3} Pa s leads to higher velocity, acceleration, and pressure at the beginning of the process but a lower ejection velocity at the moment of ejection. When the viscosity is 120×10^{-3} Pa s, there is an observable increment of velocity at the initial stage due to a pronounced viscous friction effect; however, the ejection velocity is the lowest because of the excessive viscous energy dissipation during the ejection process. It should be noted that the viscosity within the cell-extracellular medium boundary layer should also be considered in the future study even under a larger Reynolds number condition since this effect introduces a viscous force to the cell.

4.3.2 Effect of Cell-Bubble Distance. The cell response depends not only on the coating material properties but also on the operating conditions such as the cell-bubble distance and initial bubble pressure. To study this cell-bubble distance effect, Fig. 9 shows the effect of bubble distance on the cell center velocity, acceleration, and pressure under the initial pressure of 22.1 MPa and the coating viscosity of 12×10^{-3} Pa s. It is observed that the velocity, acceleration, and pressure magnitude decrease when the distance increases. Also, it is found that the profiles shift right a little bit when the cell-bubble distance increases, which indicates that it takes more time for the stress wave to reach the far away cell. It is generally expected that for the coating embedded with multiple cells, the cells close to the bubble are more susceptible to mechanical damage.

4.3.3 Effect of Initial Bubble Pressure. The initial bubble pressure also plays an important role in cell ejection, and the magnitude of initial pressure can be controlled by the laser fluence, laser

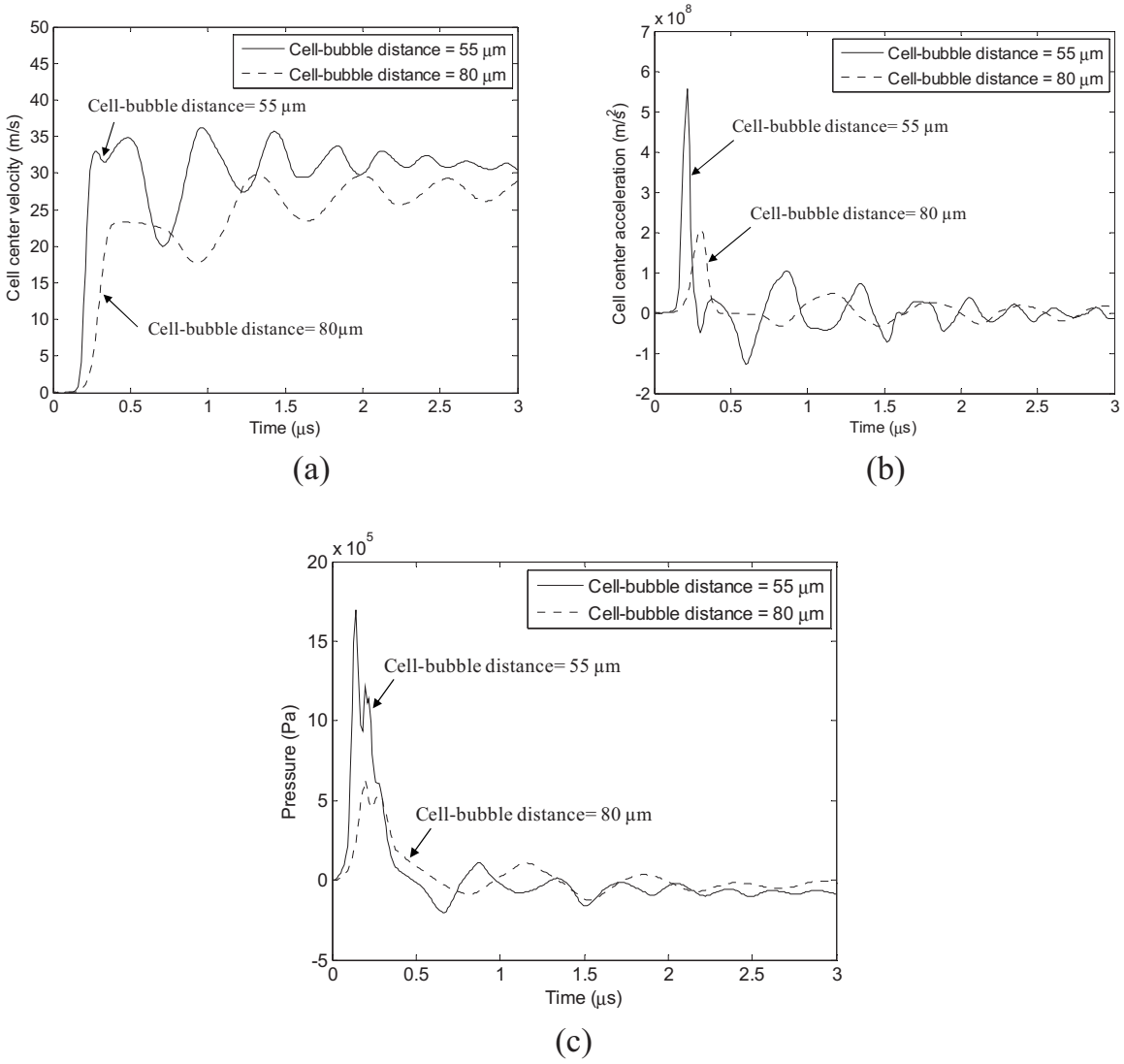

Fig. 9 (*a*) Cell center velocity, (*b*) cell center acceleration, and (*c*) cell pressure under different cell-bubble distances (the initial pressure is 22.1 MPa and the coating viscosity is 12×10^{-3} Pa s)

pulse, and energy absorption property of coating material. Generally, when the laser energy is high enough to cause the coating material to vaporize and even ionize, the cell ejection is easily caused by the bubble expansion mechanism rather than the thermoelastic stress wave. Thus, the study of how the cell responds to the initial bubble pressure is critical to mitigate the cell damage in direct writing.

Figure 10 shows the effect of initial bubble pressure on the cell center velocity, acceleration, and pressure under the coating viscosity of 12×10^{-3} Pa s and the cell-bubble distance of 55 μm. It is shown that the larger initial pressure induces a larger cell velocity, acceleration, and pressure as expected. As a result, the cell viability is adversely affected by large initial bubble pressures.

It should be noted that when the initial gas bubble pressure increases, the flow velocity magnitude increases accordingly. Thus, the inertial effect becomes dominant over the viscosity effect, and the coating material behaves more like a nonviscous flow. If it is the case, the bubble expansion-induced material motion is a nonviscous flow except within the boundary layer around the cells.

5 Discussion

The velocity, acceleration, and pressure profile, which cells experience during the ejection process in laser-assisted direct writing, has been investigated in this study. While the initial bubble formation process is not of particular interest here, the following bubble expansion-induced cell mechanical profile is studied. This modeling study first enables a quantitative understanding of the cell mechanical profile during the ejection process and offers some insight into the process-induced cell damage.

The transferred cells after direct writing are sometimes damaged and may not be viable mainly due to the pressure/stress loading studied. The effect of laser-induced pressure/stress wave on cell/tissue damage has been of interest in the laser-tissue interaction research community. It is generally recognized [8] that the laser-generated stress wave during the laser-tissue interaction may make a cell membrane permeable. As a result, molecules present in the extracellular medium may diffuse into the cytoplasm under the concentration gradient. Subsequently, the plasma membrane reseals, keeping the exogenous molecules inside the cell, which may lead to the functional cell injury [8]. The mechanisms of membrane permeabilization due to the laser-generated stress wave have been studied [31,32] but are still not elucidated yet. Furthermore, a strong stress wave may directly induce the cell membrane or other components structurally broken. The stress-induced cell damage mechanism is similar for both the laser-assisted direct writing process and the laser-tissue direct interaction. It should be pointed out that there may be some additional photomechanical

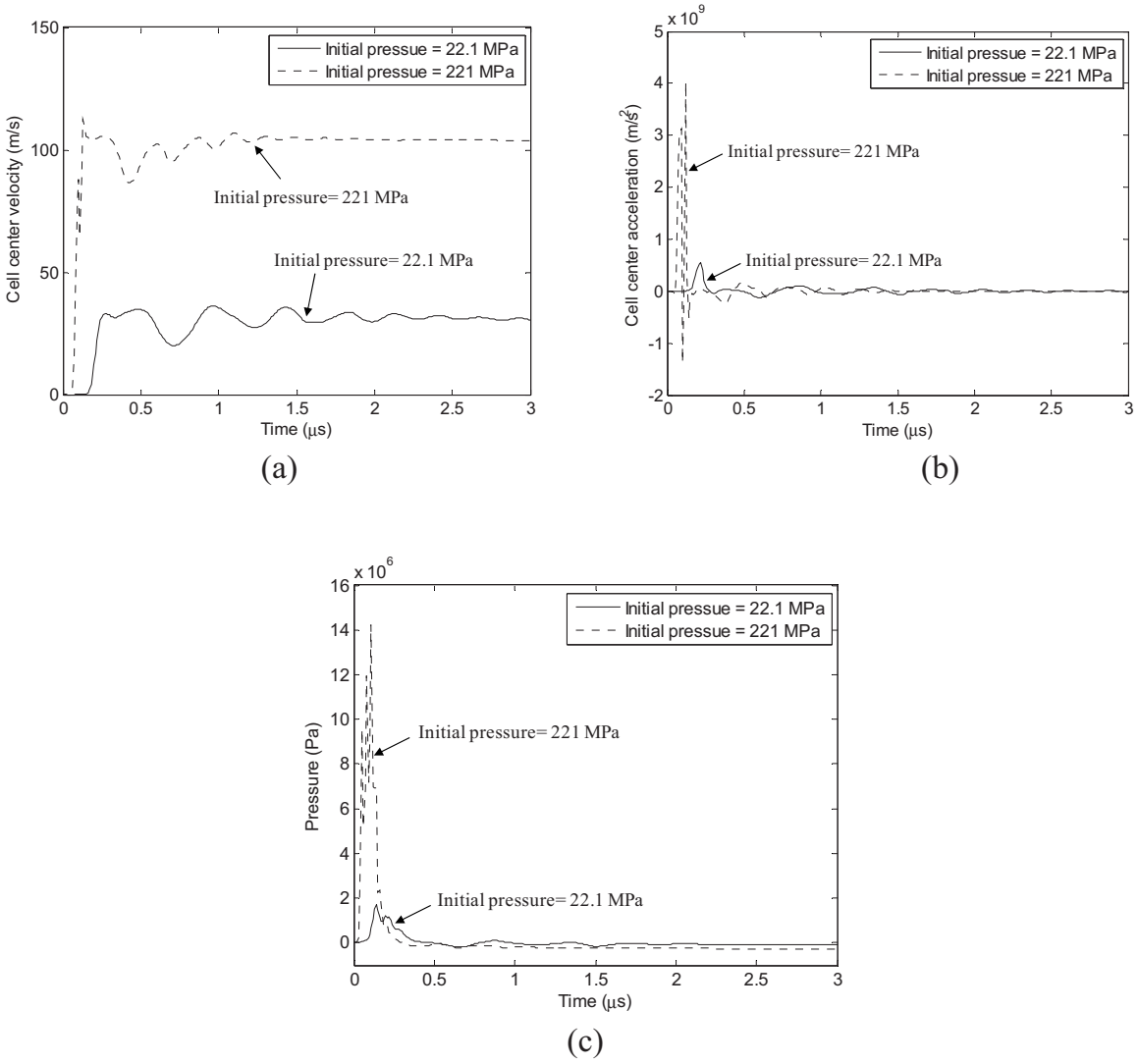

Fig. 10 (*a*) Cell center velocity, (*b*) cell center acceleration, and (*c*) cell pressure under different initial bubble pressures (the coating viscosity is 12×10^{-3} Pa s and the cell-bubble distance is 55 μm)

effect-induced thermoelastic stress waves present in laser-assisted direct writing although they are negligible when using high energy laser pulses.

The cell damage degree due to the pressure or stress depends on many different factors such as stress magnitude and/or stress duration [1,8]. Exposure of cells to high pressures may induce a high degree of membrane permeabilization and substantial damage of intercellular components, which may prevent cells from recovering from permanent injury after the removal of pressure or stress loading. It is observed in this study that the cell can first accelerate as high as 10^9 m/s^2 at the beginning period of bubble expansion and then quickly approaches zero in an oscillation manner. The acceleration rate is extremely high for a cell to survive. Fortunately, this high acceleration only lasts a very short period (about 0.1 μs), and this duration might be too short for a cell to fully respond to a very high acceleration since the cell itself is a viscoelastic material [33]. As a result, cells can still survive under a high acceleration rate if the combined effect of stress magnitude and duration is tolerable by the cell [1,3]. It was studied that the cell damage depends not only on the process-induced stress magnitudes but also on the stress duration [1]. This combined stress magnitude and duration effect on cell damage should be further modeled for cell viability control in cell direct writing.

The cell velocity information after ejection is also studied here since the impact-induced damage during landing also poses a significant challenge to achieve a high cell viability postcell transfer [1,3]. A higher ejection velocity of the formed cell droplet usually leads to a lower post-transfer cell viability [1]. This modeling study is expected to help optimize the cell direct writing process by better estimating the landing velocity for given operating direct writing conditions.

6 Conclusions and Future Work

The bubble expansion-induced cell ejection in laser-assisted cell direct writing has been carefully studied using the FEM approach in this study. Using the validated FEM approach, the evolution of cell center velocity, cell center acceleration, and pressure is studied, and the effects of coating viscosity, cell-bubble distance, and initial bubble pressure on the cell mechanical profile are further investigated during cell ejection. The main computational predictions can be drawn as follows.

1. The cell velocity oscillates initially and then smoothes out gradually with a constant ejection velocity. The cell can first accelerate as high as 10^9 m/s^2 at the beginning period of bubble expansion and then quickly approaches zero in an oscillation manner; fortunately, this high acceleration period only lasts a very short period (about 0.1 μs).

2. The cell pressure can be very high at the beginning period of bubble expansion and quickly decreases to zero in an oscillation manner as seen from the cell acceleration evolution. The cell top surface region usually experiences the highest pressure level, followed by the bottom surface and the middle regions.
3. A high viscosity can lead to an observable velocity increment at the initial stage due to the pronounced viscous friction effect, but the ejection velocity decreases because of the excessive viscous energy dissipation.
4. The pressure magnitude decreases when the cell-bubble distance is large. It is generally expected that for the coating embedded with multiple cells, the cells close to the bubble are more susceptible to mechanical damage.
5. A larger initial pressure induces a larger cell pressure as expected. As a result, the cell viability is adversely affected by large initial pressures.

As discussed before, while the MAPLE DW schematic is used in Fig. 1 for illustration, the proposed modeling approach is applicable to BioLP by assuming the energy conversion thickness negligible as well as other jet-based cell direct-write processes.

While the presented computational modeling study is validated with an analytical modeling approach here, future experimental investigation should be performed to directly validate this modeling study. Also, since the cytoplasmic membrane, cell wall, and internal structure of a cell may play an important role in determining the cell mechanical profile during ejection, future modeling study should also include the effect of cell biological structure.

Acknowledgment

The study was partially supported by the National Textile Center and the National Science Foundation (Grant No. CMMI-0747959).

References

[1] Wang, W., Huang, Y., Grujicic, M., and Chrisey, D. B., 2008, "Study of Impact-Induced Mechanical Effects in Cell Direct Writing Using Smooth Particle Hydrodynamic Method," ASME J. Manuf. Sci. Eng., **130**(2), pp. 021012-1–021012-10.
[2] Barron, J. A., Wu, P., Ladouceur, H. D., and Ringeisen, B. R., 2004, "Biological Laser Printing: A Novel Technique for Creating Heterogeneous 3-Dimensional Cell Patterns," Biomed. Microdevices, **6**(2), pp. 139–147.
[3] Ringeisen, B. R., Kim, H., Barron, J. A., Krizman, D. B., Chrisey, D. B., Jackman, S., Auyeung, R. Y. C., and Spargo, B. J., 2004, "Laser Printing of Pluripotent Embryonal Carcinoma Cells," Tissue Eng., **10**(3–4), pp. 483–491.
[4] Ringeisen, B. R., Othon, C. M., Barron, J. A., Young, D., and Spargo, B. J., 2006, "Jet-Based Methods to Print Living Cells," Biotechnology J., **1**, pp. 930–948.
[5] Lin, Y., Huang, Y., and Chrisey, D.B., 2009, "Droplet Formation in Matrix-Assisted Pulsed-Laser Evaporation Direct Writing of Glycerol-Water Solution," J. Appl. Phys., **105**, pp. 093111-1–093111-6.
[6] Odde, D. J., and Renn, M. J., 1999, "Laser-Guided Direct Writing for Applications in Biotechnology," Trends Biotechnol., **17**(10), pp. 385–389.
[7] Odde, D. J., and Renn, M. J., 2000, "Laser-Guided Direct Writing of Living Cells," Biotechnol. Bioeng., **67**, pp. 312–318.
[8] Lee, S., and Doukas, A. G., 1999, "Laser-Generated Stress Waves and Their Effects on the Cell Membrane," IEEE J. Sel. Top. Quantum Electron., **5**(4), pp. 997–1003.
[9] Vogel, A., and Venugopalan, V., 2003, "Mechanisms of Pulsed Laser Ablation of Biological Tissues," Chem. Rev. (Washington, D.C.), **103**, pp. 577–644.
[10] Vogel, A., Busch, S., and Parlitz, U., 1996, "Shock Wave Emission and Cavitation Bubble Generation by Picosecond and Nanosecond Optical Breakdown in Water," J. Acoust. Soc. Am., **100**(1), pp. 148–165.
[11] Tomita, Y., Tsubota, M., and An-naka, N., 2003, "Energy Evaluation of Cavitation Bubble Generation and Shock Wave Emission by Laser Focusing in Liquid Nitrogen," J. Appl. Phys., **93**(5), pp. 3039–3048.
[12] Glinsky, M. E., Bailey, D. S., London, R. A., Amendt, P. A., Rubenchik, M. R., and Strauss, M., 2001, "An Extended Rayleigh Model of Bubble Evolution," Phys. Fluids, **13**(1), pp. 20–31.
[13] Byun, K. T., and Kwak, H. Y., 2004, "A Model of Laser-Induced Cavitation," Jpn. J. Appl. Phys., Part 1, **43**(2), pp. 621–630.
[14] Brujan, E. A., and Vogel, A., 2006, "Stress Wave Emission and Cavitation Bubble Dynamics by Nanosecond Optical Breakdown in a Tissue Phantom," J. Fluid Mech., **558**, pp. 281–308.
[15] Friedman, M., Strauss, M., Amendt, P., London, R. A., and Glinsky, M. E., 2002, "Two-Dimensional Rayleigh Model for Bubble Evolution in Soft Tissue," Phys. Fluids, **14**(5), pp. 1768–1780.
[16] Lokhandwalla, M., and Sturtevant, B., 2001, "Mechanical Haemolysis in Shock Wave Lithotripsy (SWL): I. Analysis of Cell Deformation Due to SWL Flow-Fields," Phys. Med. Biol., **46**, pp. 413–437.
[17] 2007, LS-DYNA Keyword User's Manual, Livermore Software Technology Corporation, Livermore, CA.
[18] Stammen, J. A., Williams, S., Ku, D. N., and Guldberg, R. E., 2001, "Mechanical Properties of a Novel PVA Hydrogel in Shear and Unconfined Compression," Biomaterials, **22**, pp. 799–806.
[19] Vijayasekaran, S., Fitton, J. H., Hicks, C. R., Chirila, T. V., Crawford, G. J., and Constable, I. J., 1998, "Cell Viability and Inflammatory Response in Hydrogel Sponges Implanted in the Rabbit Cornea," Biomaterials, **19**(24), pp. 2255–2267.
[20] Young, C. D., Wu, J. R., and Tsou, T. L., 1998, "High-Strength, Ultra-Thin and Fiber-Reinforced pHEMA Artificial Skin," Biomaterials, **19**, pp. 1745–1752.
[21] Wang, T., Turhan, M., and Gunasekaran, S., 2004, "Selected Properties of pH-Sensitive, Biodegradable Chitosan-Poly (Vinyl Alcohol) Hydrogel," Polym. Int., **53**, pp. 911–918.
[22] Nam, K., Watanabe, J., and Ishihara, K., 2005, "Network Structure of Spontaneously Forming Physically Cross-Link Hydrogel Composed of Two-Water Soluble Phospholipid Polymers," Polymer, **46**, pp. 4704–4713.
[23] Roeder, B. A., Kokini, K., Sturgis, J. E., Robinson, J. P., and Voytik-Harbin, S. L., 2002, "Tensile Mechanical Properties of Three-Dimensional Type I Collagen Extracellular Matrices With Varied Microstructure," ASME J. Biomech. Eng., **124**, pp. 214–222.
[24] Drury, J. L., Dennis, R. G., and Mooney, D. J., 2004, "The Tensile Properties of Alginate Hydrogels," Biomaterials, **25**, pp. 3187–3199.
[25] Lin, D. C., Yurke, B., and Langrana, N. A., 2004, "Mechanical Properties of a Reversible, DNA-Crosslinked Polyacrylamide Hydrogel," ASME J. Biomech. Eng., **126**, pp. 104–110.
[26] Lim, C. T., Zhou, E. H., and Quek, S. T., 2006, "Mechanical Models for Living Cells—A Review," J. Biomech., **39**, pp. 195–216.
[27] Breuls, R. G. M., Bouten, C. V. C., Oomens, C. W. J., Bader, D. L., and Baaijens, F. P. T., 2003, "A Theoretical Analysis of Damage Evolution in Skeletal Muscle Tissue With Reference to Pressure Ulcer Development," ASME J. Biomech. Eng., **125**, pp. 902–909.
[28] Ohayon, J., and Tracqui, P., 2005, "Computation of Adherent Cell Elasticity for Critical Cell-Bead Geometry in Magnetic Twisting Experiments," Ann. Biomed. Eng., **33**(2), pp. 131–141.
[29] Plesset, M. S., and Prosperetti, A., 1977, "Bubble Dynamics and Cavitation," Annu. Rev. Fluid Mech., **9**, pp. 145–185.
[30] Gerstman, B. S., Thompson, C. R., Jacques, S. L., and Rogers, M. E., 1996, "Laser Induced Bubble Formation in the Retina," Lasers Surg. Med., **18**, pp. 10–21.
[31] McAuliffe, D. J., Lee, S., Flotte, T. J., and Doukas, A. G., 1997, "Stress-Wave-Assisted Transport Through the Plasma Membrane In Vitro," Lasers Surg. Med., **20**, pp. 216–222.
[32] Lee, S., McAuliffe, D. J., Zhang, H., Xu, Z., Taitelbaum, J., Flotte, T. J., and Doukas, A. G., 1997, "Stress-Wave-Induced Membrane Permeation of Red Blood Cells is Facilitated by Aquaporins," Ultrasound Med. Biol., **23**, pp. 1089–1094.
[33] Kasza, K. E., Rowat, A. C., Liu, J., Angelini, T. E., Brangwynne, C. P., Koenderink, G. H., and Weitz, D. A., 2007, "The Cell as a Material," Curr. Opin. Cell Biol., **19**, pp. 101–107.